3

Knockdown of filaggrin does not affect lipid organization and composition in stratum corneum of reconstructed human skin equivalents

Vincent van Drongelen*, Mariam Alloul-Ramdhani*,
Mogbekeloluwa O. Danso, Arnout Mieremet, Aat Mulder,
Jeroen van Smeden, Joke A. Bouwstra and Abdoelwaheb El Ghalbzouri

**these authors share first authorship*

Experimental Dermatology 2013 Dec;22(12):807-12

Abstract

Human skin mainly functions as an effective barrier against unwanted environmental influences. The barrier function strongly relies on the outermost layer of the skin, the stratum corneum (SC), which is composed of corneocytes embedded in an extracellular lipid matrix. The importance of a proper barrier function is shown in various skin disorders such as atopic dermatitis (AD), a complex human skin disorder strongly associated with filaggrin (FLG) null mutations, but their role in barrier function is yet unclear. To study the role of FLG in SC barrier properties in terms of SC lipid organization and lipid composition, we generated an N/TERT based 3D-skin equivalent (NSE) after knockdown of FLG with shRNA. In these NSEs, we examined epidermal morphogenesis by evaluating the expression of differentiation markers keratin 10, FLG, loricrin and the proliferation marker ki67. Furthermore, the SC was extensively analysed for lipid organization, lipid composition and SC permeability. Our results demonstrate that FLG knockdown (FLG-KD) did not affect epidermal morphogenesis, SC lipid organization, lipid composition and SC permeability for a lipophilic compound in NSEs. Therefore, our findings indicate that FLG-KD alone does not necessarily affect the functionality of a proper barrier function.

Introduction

The barrier function strongly relies on the outermost layer of the skin, the stratum corneum (SC), which is composed of corneocytes embedded in an extracellular lipid matrix. Since the extracellular SC lipid matrix forms a continues pathway between the corneocytes, it has been suggested to act as an important penetration pathway through the SC[1]. This lipid matrix is composed of ceramides (CERs), cholesterol (CHOL) and free fatty acids (FFAs) which are organized into lipid layers referred to as lamellar phases[2-4]. X-ray diffraction studies revealed that human skin contains two lamellar phases, the long periodicity phase (LPP) and the short periodicity phase (SPP), with a repeat distance of approximately 13 and 6 nm, respectively[5;6]. Within the lamellar phases, the lipids are organized in a certain density, referred to as the lateral packing, either orthorhombic (very dense), hexagonal (dense) or liquid (loose)[5-9] (Figure S1). Atopic dermatitis (AD) is a common inflammatory skin disorder characterized by impaired skin barrier function that affects over 15% of Caucasian children and 2-10% adults[10]. AD skin is characterized by increased transepidermal water loss (TEWL), decreased hydration and increased permeability for compounds such as sodium lauryl sulphate[10-13] . To date, the strong association between filaggrin (FLG) null mutations and AD is one of the most robust genotype linkage observed in complex human genetic disorders, but the effect of such FLG mutations on skin barrier is not yet fully understood[14-18]. Recently, it was demonstrated that SC lipid organization and CER composition correlated with the impaired skin barrier function in AD[19].

The clinical phenotype of AD is the result of complex interactions between environmental and genetic factors that results in an inflammatory response and impaired skin barrier function. Therefore the single contribution of reduced FLG expression due to FLG null mutations on skin barrier (dys-)function is difficult to assess *in vivo.* The discovery that Th2 cytokines such as IL-4, IL-13 and IL-31 affect FLG expression, add further complexity for studying the role of FLG in the barrier function of AD patients *in vivo*[20;21]. In the present study we therefore generated a reproducible full thickness model using the N/TERT cell line after shRNA mediated knockdown of FLG. This approach allows us to elucidate the single contribution of FLG on epidermal morphogenesis and SC barrier properties *in vitro*. We chose for reconstructed human skin equivalents as these models reproduce many features that are present in *ex vivo* skin concerning the lipid properties and most of the barrier proteins[22]. In a previous study, Mildner and colleagues showed that siRNA mediated knockdown of FLG in human skin equivalents (HSEs) results in increased epidermal uptake of a fluorescent dye[23]. However, whether FLG deficiency affects permeation across the SC and whether FLG deficiency affects SC lipid organization and SC lipid composition was not studied. Using an N/TERT based human skin equivalent (NSE), we extensively analyzed various SC barrier properties, including lamellar lipid organization, lateral lipid packing, lipid composition and permeability.

Material and Methods

Cell culture

Primary human fibroblasts were obtained from surplus skin from adult donors undergoing mammary or abdominal surgery and were established as described earlier[23;24]. For all experiments, fibroblasts cultured at 37°C and 5% CO_2 from passage 2-5 were used for generation of NSEs. The N/TERT keratinocyte cell line was purchased from Harvard Medical School (USA) and cultured in keratinocyte serum free medium (KSFM medium, Invitrogen), supplemented with 25 µg/ml BPE, 0.4 mM $CaCl_2$ 0.2ng/ml hEGF, 100 U/ml penicillin and 100 µg/ml Streptomycin (Invitrogen).

Generation of stable N/TERT cell lines

N/TERT cells were transfected with pLKO.1-puro plasmid containing shRNA against filaggrin using the Amaxa human keratinocyte nucleofector kit (Lonza, Breda, the Netherlands) according manufacturer's protocol using program T-07. Plasmids containing shRNA against filaggrin (TRCN0000083680) obtained from the Mission library from Sigma-Aldrich was used. As a control we used cells transfected with empty pLKO.1-puro plasmid (Mock, TRC1.5-SHC001) and untransfected N/TERT. Transfected cells were cultured similar to N/TERT cells except for the addition of puromycin to the KSFM medium (1 ug/ml).

Dermal Equivalents

Dermal equivalents were generated as described earlier[25]. Briefly, 1 ml of cell-free collagen (1mg/ml) was pipetted into a 6 well-filter insert (Corning Life Sciences). After polymerization, 3 ml of fibroblast populated ($0.4x10^5$ fibroblasts/ml) collagen (2 mg/ml) was pipetted onto the polymerized collagen layer. After polymerization the dermal equivalents were submerged in medium consisting of DMEM, 5% FCS and 1% penicillin/streptomycin. Medium was refreshed twice a week.

Generation of NSEs

NSEs were generated by seeding $5x10^5$ N/TERT cells onto a dermal equivalent. These NSEs were cultured in medium containing 5% FCS for 2 days, after which the FCS concentration was reduced to 1% for an additional day. Next, NSEs were lifted to the air-liquid interface and cultured for 2 weeks with FCS-free medium supplemented with 2M L-serine, 10 mM L-carnitine, 1 µM DL-α- tocopherol-acetate, 50 µM ascorbic acid, a free fatty acid supplement which contained 25 µM palmitic acid, 30 µM linoleic acid and 7 µM arachidonic acid and $2.4x10^{-5}$ M bovine serum albumin. Culture medium was refreshed twice a week.

Morphology and immunohistochemistry

NSEs were fixed in 4% formaldehyde and embedded in paraffin. Morphological analysis was performed on 5 µm sections through haematoxylin and eosin staining. Immunohistochemical analyses was performed using the streptavidin-biotin-peroxidase system (GE Healthcare, Buckinghamshire, UK), according manufacturer's instructions. Staining's were visualized with 3-amino-9-ethylcarbazole (AEC), counterstained with haematoxylin and sealed with Kaisers glycerin. The primary and secondary antibodies are given in supplementary Material and Methods.

Estimation of proliferation index

To estimate the proliferation index, the number of Ki67 positive nuclei in a total number of 100 basal cells (x100%) was determined on 3 locations per slide for three different experiments. Data represent mean and standard deviation.

Determination of the number of stratum corneum layers

The layers of the stratum corneum were counted as described previously[26]. For details see supplementary Material and Methods. Data represent mean and standard deviation.

RNA isolation, cDNA synthesis and qPCR

RNA was isolated from the epidermis of NSEs using the RNeasy kit (Qiagen) according manufacturer's instructions. Prior to RNA isolation, the samples underwent a proteinase K treatment. cDNA was generated using the iScript cDNA synthesis kit (BioRad, Veenendaal, The Netherlands) according manufacturer's instructions. PCR reactions were based on the SYBR Green method (BioRad) using the CFX384 system (BioRad). Expression analysis was performed using CFX software using the ΔΔCt method using the reference gene β-2-microglobulin. Data represent mean and standard deviation of 3 different experiments.

Protein isolation and Western blot

Proteins were isolated from the epidermis using Tissue Protein Extraction Reagent (T-PER) supplemented with protease inhibitor cocktail and HALT™ phosphatase inhibitors (Thermo Scientific, Etten-Leur, the Netherlands). For western blot details see supplementary Material and Methods.

Stratum corneum isolation

The SC from NSEs was isolated as described earlier[27]. Briefly, NSEs were incubated overnight on filter paper with 0.1% trypsin in 4˚C. After 30 minutes incubation at 37˚C, SC was mechanically separated from the NSEs and subsequently washed with 1 ug/ml trypsin inhibitor (Sigma, Zwijndrecht, The Netherlands) and demineralized water. SC samples were air dried at room temperature and stored under Argon gas over silica gel in the dark.

Fourier transformed infrared spectroscopy and small angle X-ray diffraction
Fourier transform infrared spectroscopy (FTIR) and small angle X-ray diffraction (SAXD) were performed as described earlier[22]. For details see supplementary Material and Methods. All measurements were performed using three SC samples of all NSE types. Data represent mean and standard deviation.

Lipid extraction
SC lipids were extracted according to a modified Bligh and Dyer procedure as described in the supplementary Material and Methods and elsewhere[22;28]. To obtain sufficient lipids for quantification, lipid extracts from 2-4 NSEs from each donor were pooled.

HPTLC lipid analysis
Extracted SC lipids were quantified using HPTLC. The solvent system to separate the lipids is described elsewhere[29]. Co-chromatography of serial dilutions of a standard mixture was used to identify and quantify each lipid class. HPTLC details and ceramide nomenclature is given in supplementary Material and Methods according to terminology of Motta *et al.*, and Masukawa *et al.*[30;31]. Data represent mean and standard deviation of 2 different experiments.

LC/MS lipid analysis
The CERs and FFAs in pooled lipid extracts of the NSEs were analyzed by LC/MS according to the method described in the supplementary Material and Methods and elsewhere (van Smeden *et al.*, submitted). Quantification of FFAs was performed using lipid extracts of SC from two experiments for each NSE type. Data represent mean and standard deviation.

Permeability studies
In vitro permeation studies were performed with butyl para-aminobenzoic acid (butyl-PABA) as described earlier with small adjustments[32]. The donor compartment was filled with 1.5 ml butyl-PABA solution (50 μg/ml butyl-PABA) in acetate buffer (pH 5.0). The acceptor compartment consisted of PBS (pH 7.4), perfused at a flow rate of 1.5 ml/hr. Permeability studies were performed with at least 6 SC sheets of all NSE types. Data represent mean and standard deviation.

Statistical analysis
Statistical significance was determined using the two-tailed Student's *t*-test. The permeability studies were analyzed using ANOVA.

Results

Filaggrin knockdown does not affect epidermal morphogenesis of NSEs

Stable knockdown of filaggrin (FLG-KD) was obtained through electroporation of FLG specific shRNA in N/TERT cells selected by puromycin, which were subsequently used for the generation of NSEs. After culturing the NSEs for 14 days air-exposed, a significant reduction of approximately 85% of FLG mRNA expression was present in FLG-KD NSEs, when compared to the control (Mock) (Figure 1a). Both western blot and immunohistochemical analysis show a strong decrease in FLG protein expression and reduced expression in the stratum granulosum, respectively (Figure 1b, c). All NSE types showed a fully developed epidermis consisting of all epidermal layers (Figure 1c). Additionally, the expression of the early differentiation marker K10 in the suprabasal layers and the late differentiation marker loricrin in the stratum granulosum indicated a normal differentiation program, irrespective of FLG-KD (Figure 1c). Determination of the proliferation index by Ki67 showed that FLG-KD did not affect basal cell proliferation (Figure 1d). To evaluate whether FLG-KD affected SC thickness, a saffranin red staining was used which revealed that the number of layers in the SC was not affected by FLG-KD (Figure 1e).

SC lamellar lipid organization is not altered after FLG-KD in NSEs

After evaluation of epidermal development in NSEs, we determined whether FLG-KD affected SC lipid organization. Since presence of the LPP is an important determinant in skin barrier function, SAXD was used to evaluate the lamellar organization. FLG-KD NSEs displayed the presence of the 1st, 2nd, and 3rd order diffraction peaks, indicated the presence of the LPP (Figure 2a). The average repeat distance of the LPP for the N/TERT, Mock and FLG-KD NSEs was 12.1 nm (± 0.4 nm), 12.3 nm (± 0.7 nm) and 12.1 (± 0.4 nm) respectively (Figure 2a), indicating that FLG-KD did not affect the presence of the LPP nor its repeat distance. In addition to the 1st, 2nd, and 3rd order diffraction peaks, occasionally a small extra peak was observed in the NSE curves.

FLG-KD in NSEs did not affect the lateral packing of the SC lipids

The lateral packing in the SC of the NSEs was examined by monitoring the CH_2 rocking band vibrations in a FTIR spectrum. When lipids are in an orthorhombic packing the CH_2 rocking band consists of two vibrations at 719 and 730 cm^{-1}, whereas a hexagonal lateral packing results in a single vibration at 719 cm^{-1}. A detailed explanation of FTIR and its usage for evaluation of the lateral packing in the SC of HSEs is described elsewhere[22]. Only a vibration at 719 cm^{-1} was observed for all three NSEs, demonstrating that FLG-KD NSEs show a hexagonal lateral packing similar to the control (Mock) and N/TERT (Figure S2a).

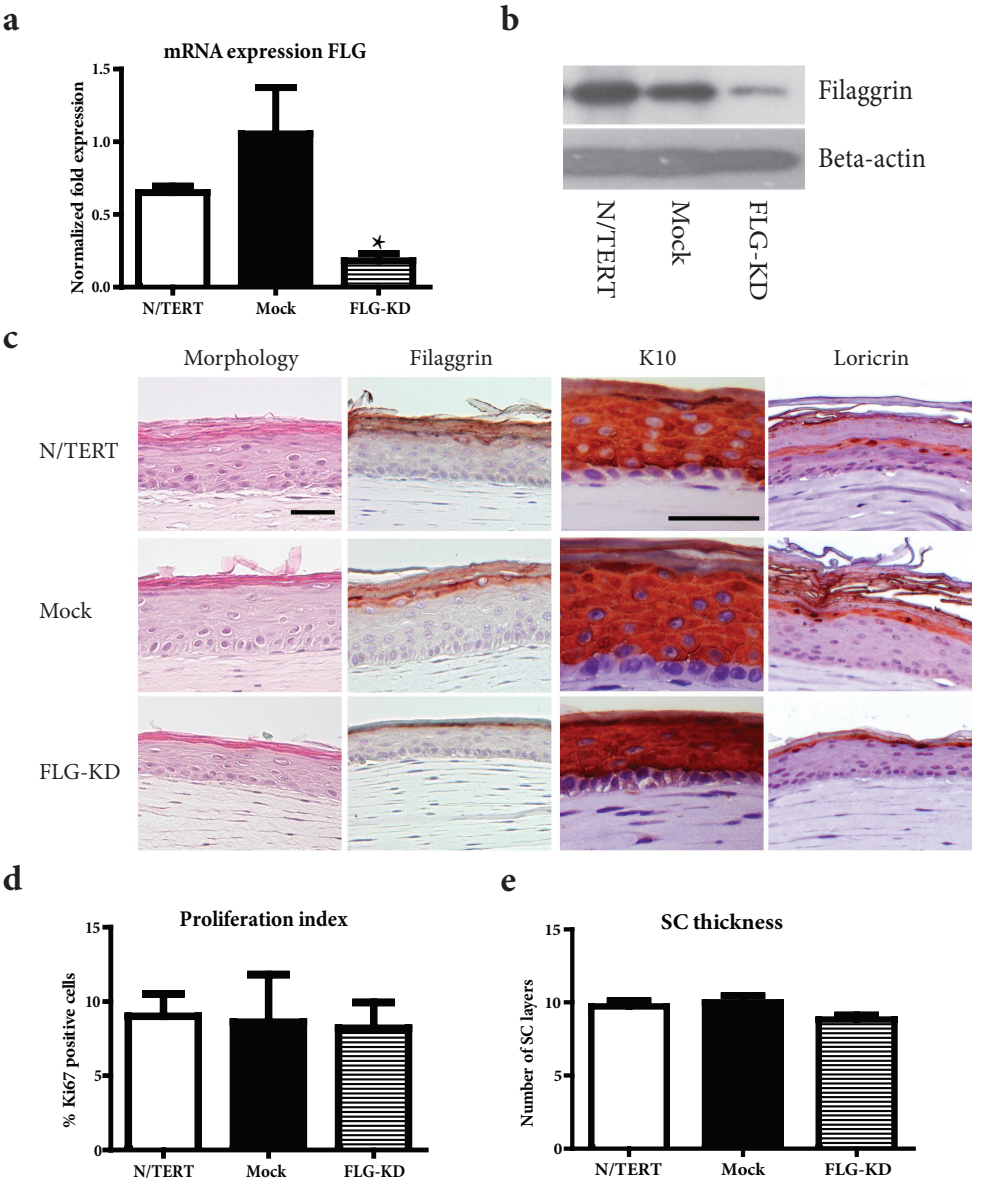

Figure 1: Filaggrin knockdown in 14 days air-exposed NSEs. (a) qPCR analysis after FLG-KD. FLG mRNA expression in NSEs was reduced with approximately 85% after nucleofection with FLG-specific shRNA, compared to the control (Mock). Data represent the mean + SD of three independent experiments. (b) Western blot analysis for filaggrin. FLG-KD NSEs show reduced FLG protein expression after culturing at the air-liquid interface for 14 days. (c) Immunohistochemical staining for FLG, keratin 10 and loricrin. Reduced FLG expression was present in the stratum granulosum of FLG-KD NSEs, but did not affect the expression of keratin 10 and loricrin. Scale bars: 50 µm. (d) proliferation index after Ki67 revealed that FLG-KD did not affect epidermal proliferation. Data represent the mean + SD of three independent experiments. (e) Saffranin red staining for the evaluation of the number of SC layers showed that FLG-KD did not affect the number of SC layers of NSEs after 14 days air exposed culturing. Data represent mean + SD of 5 independent experiments.

To evaluate at which temperatures the lipid domains transform into a liquid phase, the CH_2 symmetric stretching was assessed (Figure S2b). This provides information about the conformational ordering of the lipids. Lipids in a crystalline phase (orthorhombic or hexagonal packing) display a CH_2 symmetric stretching below 2850 cm^{-1}. In a liquid phase the conformational disordering is high, resulting in symmetric stretching vibrations between 2852 - 2854 cm^{-1}. At 32°C, FLG-KD NSEs displayed a CH_2 stretching frequency of 2850.8 ± 0.8 cm^{-1} comparable to the CH_2 stretching frequency of the Mock (2850.7 ± 0.6 cm^{-1}) and N/TERT (2850.3 ± 0.2 cm^{-1}) (Figure S1c). Since the order-disorder transition occurs over a temperature range between 0 and 90°C, the midpoint temperature of this transition was determined. This midpoint order-disorder transition of the FLG-KD NSEs was comparable to the Mock and N/TERT NSEs (Figure S2c)

FLG-KD did not alter SC lipid composition in NSEs

We quantified the SC lipid composition of the NSEs by HPTLC, which revealed a similar SC lipid profile for the N/TERT, Mock and FLG-KD NSEs (Figure 2b). The amount of lipids as a percentage of total SC weight was determined by weighing SC before and after lipid extraction. FLG-KD did not affect the percentage weight of lipids in the SC (Figure 2c) and quantification of the different lipid classes showed similar levels of CHOL, CER and FFA present in SC of all NSEs (Figure 2d, e)). FLG-KD did not affect the presence of the different CER subclasses, as the relative level of each CER subclass was not significantly different for all three NSEs (Figure 2e). Additionally, FLG-KD did not significantly affect the ratio between the total EO ceramides (EO CERs, acylceramides) and non EO ceramides (non EO CERs, a-hydroxy and non-hydroxy ceramides) (Figure 2f). Subsequently, SC lipid composition was evaluated in more detail using liquid chromatography/mass spectrometry (LC/MS). HPTLC can be used to separate 9 CER subclasses, while with LC/MS 12 CER subclasses and their chain length distribution can be detected[33]. LC/MS showed that FLG-KD did not affect the presence of the 12 CER subclasses and their chain length distribution by FLD-KD (Figure S3).

Since FFA chain length is important for CER chain length and for SC lipid organization, LC/MS was performed to evaluate whether the FFA composition was affected by FLG-KD. All NSEs displayed the presence of saturated FFAs and monounsaturated FFAs (MUFAs) (Figure 3a-c). FFA chain length distribution varied between C16:0 and C28:0 and C16:1 and C32:1 for the saturated FFAs and MUFAs respectively in all NSEs, indicating that FLG-KD did not affect FFA saturation nor chain length distribution. In addition, hydroxy FFAs were detected, but due to their low abundance could not be visualised in the plot. Quantification of the relative amounts of the various FFA classes revealed that FLG-KD did not affect the distribution of the FFAs (Figure 3d and S4). Also the ratio of the long chain fatty acids (LCFA, C16-C21) and very long chain fatty acids (VLCFAs, C22-C38) was not affected by FLG-KD (Figure 3e). Quantification of all FFAs is shown in Figure S4.

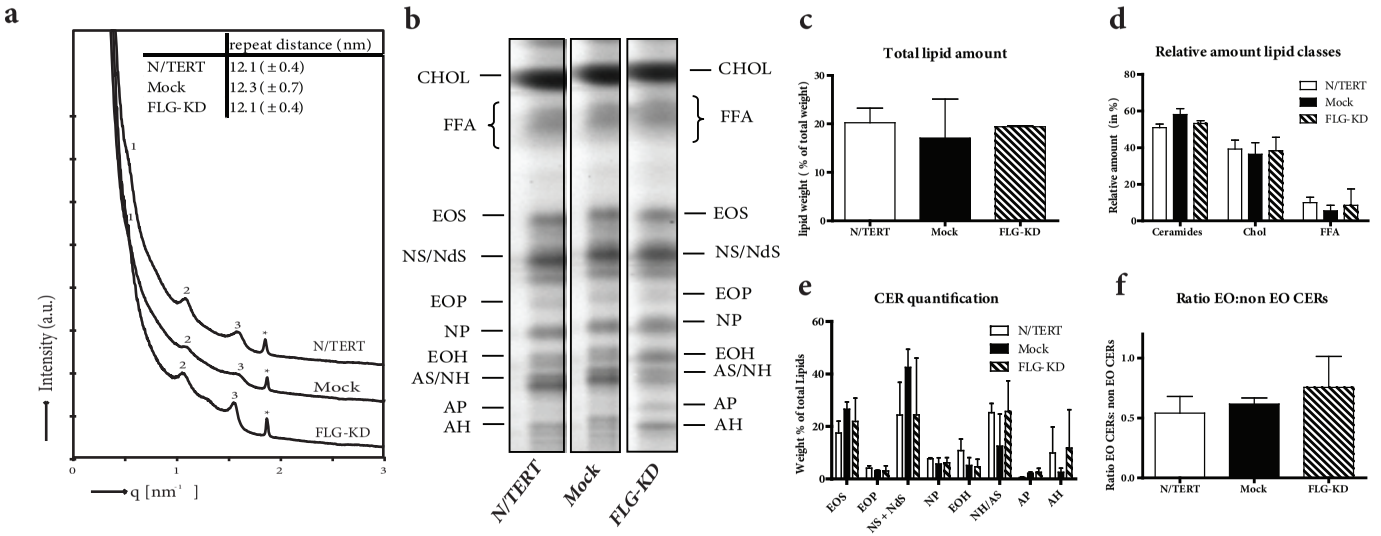

Figure 2: Effect of FLG-KD on the SC lamellar lipid organisation and SC lipid composition. (a) Representative SAXD profiles for the N/TERT (untreated), Mock and FLG-KD NSEs are shown. The first-, second- and third order diffraction peaks of the LPP are indicated by 1, 2 and 3 respectively. All NSEs show the presence of the LPP and of phase-separated cholesterol (indicated with *). The corresponding repeat distance for the LPP for the N/TERT, Mock and FLG-KD NSEs was 12.1 nm (± 0.4 nm), 12.3 nm (± 0.5 nm) and 12.0 (± 0.4 nm) respectively. Data represent mean ± SD of 3 independent experiments. (b) SC lipid composition of all three NSEs. CHOL, FFA, ceramide nomenclature according to Motta *et al.* and Masukawa *et al.*[30;31]. (c) Lipid in weight percentage of the total SC weight. (d) Relative levels of the different lipid classes in the different NSEs. (e) CER subclasses in the SC of the different NSEs. (f) Ratio EO CER and non EO CERs. FLG-KD did not affect the CER composition as determined by HPTLC. Data represent mean + SD of 2 independent experiments.

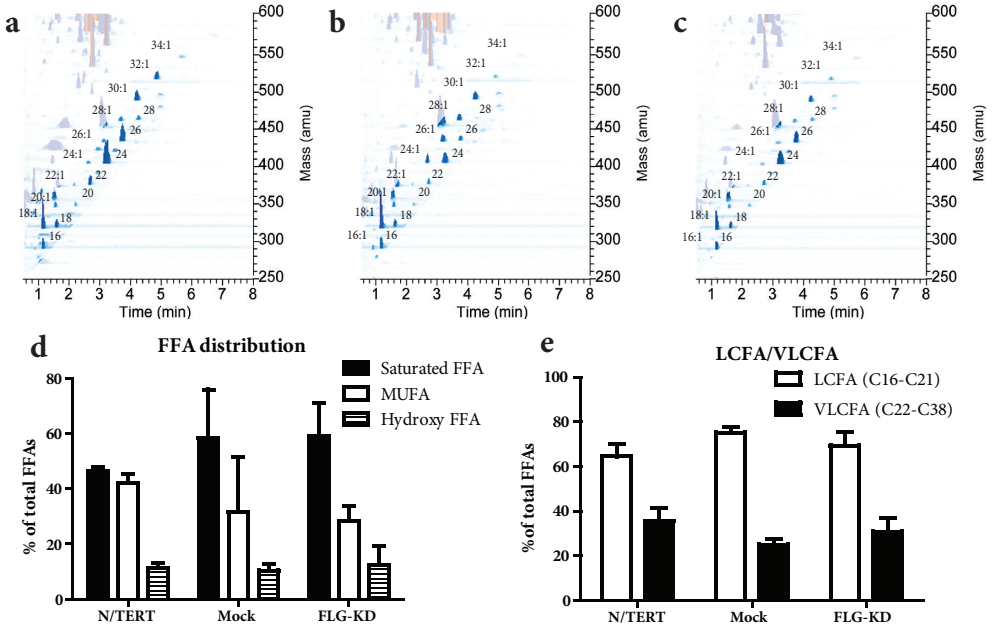

Figure 3: Liquid chromatography/mass spectrometry (LC/MS) chromatograms. Three-dimensional multi-mass LC/MS chromatogram of the FFAs present in SC lipid extracts from (a) N/TERT, (b) Mock and (c) FLG-KD NSEs. All NSEs display the presence of saturated and monounsaturated FFAs with similar chain length distribution ranging between C16:0 and C28:0 and C16:1 and C32:1 indicating that FLG-KD did not affect the FFA saturation nor chain length distribution. (d) relative distribution of the different FFA subclasses. The distribution of the FFA subclasses was not affected by FLG-KD. (e) relative distribution of the long chain fatty acids (LCFAs) and the very long chain fatty acids (VLCFAs). FLG-KD NSEs showed similar distribution of the LCFAs and VLCFAs. Total amount of all FFAs was set at 100%. Data represent mean + SD of 2 independent experiments.

SC permeability was not increased after FLG-KD in NSEs

After investigation of the SC lipid organization and composition, we examined the SC barrier function after FLG-KD. Therefore, diffusion of a lipophilic model compound, butyl-PABA, through the SC was evaluated. The flux of butyl-PABA through the SC of the three NSEs is similar and not affected by FLG-KD (Figure 4), clearly demonstrating that FLG-KD did not affect SC permeability for butyl-PABA.

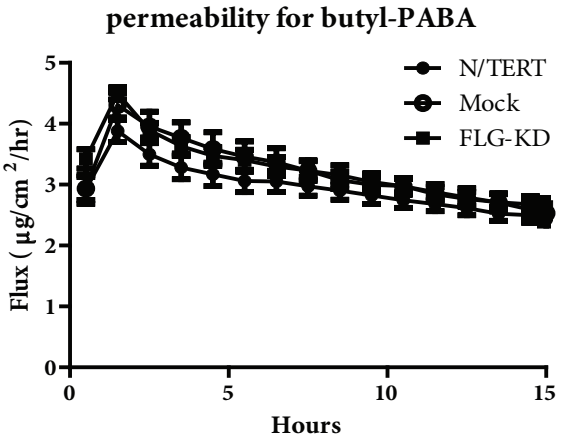

Figure 4: SC permeability for butyl-PABA after FLG-KD. To investigate the SC permeability, we used butyl-PABA as a model drug. The diffusion profiles for butyl-PABA were similar for the untreated N/TERT, Mock and FLG-KD NSEs, indicating that FLG-KD did not affect the permeability for this compound. Data represent the mean ± SEM of at least 6 measurements from three different experiments.

Discussion

FLG null mutations are a well-known predisposing factor for development of AD, an inflammatory skin disorder characterized by a defective skin barrier function. Since AD is the result of complex interactions between genetic and environmental factors that result in inflammation, the single contribution of FLG null mutations on skin barrier (dys-)function is difficult to assess *in vivo.* Especially the discovery that cytokines, e.g. Il-4 and IL-13, have been shown to reduce FLG expression and that such cytokines affect SC lipid composition, add further complexity for studying the role of FLG in barrier function in AD *in vivo*[20;21;34]. To study the effect of FLG deficiency on epidermal development and SC barrier properties, we generated NSEs after shRNA-mediated knockdown of filaggrin. These FLG-KD NSEs were studied extensively for their barrier properties, including SC lipid organization, lipid composition and permeability.

FLG-KD did not affect epidermal development in our NSEs. Differentiation was not affected by FLG-KD, in line with previous studies that used siRNA oligonucleotides or lentiviral transduction for FLG-KD[23;34]. In addition, FLG-KD did not affect epidermal proliferation in NSEs. Earlier reports on the role of FLG on epidermal proliferation are contradicting. A recent study showed no effect on epidermal thickening using a raft culture system after FLG-KD through adenoviral transfection, while others showed epidermal hyperproliferation in primary keratinocytes using lentiviral miR constructs to target pro-FLG[34;35]. Such differences might be explained by differences in the established skin models, cell origin and/or experimental set-up.

Since the SC is the principle layer for skin barrier function and FLG is an important barrier protein, we mainly focused on this layer to evaluate the effect of FLG-KD on various barrier properties. Reduced expression of FLG has been suggested to result in an increase in pH and thereby affect the activity of various enzymes involved in lipid metabolism[36]. Thereby FLG-KD in an NSE might result in alterations in SC lipid composition as seen in AD patients. Our analysis concerning the SC lipid composition using quantitative HPTLC and LC/MS show that there is no effect of FLG-KD on the SC lipid composition of NSEs. This indicates that FLG-KD alone is not sufficient to affect the SC lipid composition and that other factors then FLG, e.g. inflammation, might be involved. This is in agreement with *in vivo* studies that showed that there is no relation between FLG null mutations and the SC lipid composition and organization[19;37].

Studies using the flaky tail mouse model containing a homozygous frameshift mutation in the FLG gene, have shown an enhanced percutaneous allergen priming and an increased sensitivity to epicutanous application of ovalbumin[38;39]. However, whether these results are due to an increased penetration or increased response in the viable skin is not yet known.

Furthermore, the stratum corneum barrier properties of these mice have not yet been investigated., in addition, a recent study showed that the development of skin lesions in flaky tail mice was dependent on the adaptive immunity rather than the FLG mutations since these mice without T and B cells did not develop lesions[40].

In agreement with the SC lipid composition, SAXD results showed that FLG-KD did not affect the lamellar organisation in SC. The LPP was prominently present and no effect on the repeat distance of the LPP was observed. FTIR results showed that the lateral packing and the conformational ordering were also not affected by FLG-KD. As reported earlier for HSEs generated with primary keratinocytes, SC from NSEs mainly show a hexagonal lateral packing and was not affected by FLG-KD[22].

Since the extracellular lipid matrix forms a continuous pathway between the impermeable corneocytes, it has been suggested to act as an important penetration pathway through the SC. We therefore used a lipophilic compound, butyl-PABA, which has previously been described for its usage in *in vitro* permeability studies[32]. Our findings clearly show that FLG-KD did not affect SC permeability of NSEs for this compound. These studies are different from those reported by Mildner *et al.* who showed an increased epidermal uptake for the fluorescent dye Luciferase yellow after FLG-KD[23]. While these studies provide information about the effect of FLG-KD on amount of fluorescent dye present in the epidermis after a predetermined time interval, our studies show that FLG-KD did not affect the permeation of butyl-PABA across the SC as function of time. Furthermore, the observed differences may also be explained by the compound properties (e.g. lipophilic versus hydrophilic) and/or by differences in protocols to establish knockdown of filaggrin and the subsequent generation of HSEs.

In conclusion, we here show that FLG-KD does not affect epidermal morphogenesis, SC lipid organization, lipid composition and SC permeability in NSEs. The role of FLG in AD pathology remains unclear but our results indicate that FLG does not play a role in the SC lipid organization and composition, in line with recent publications for AD patients[19]. Other recent studies have shown that complete FLG deficiency in ichtyosis vulgaris (IV) was associated with only moderate changes in epidermal permeability barrier function in terms of TEWL, skin hydration and surface pH, changes that were absent in IV patients that were heterozygous for FLG null mutations[41;42]. While these studies focussed on other barrier parameters, they underline the findings presented in this study that FLG deficiency alone does not result in barrier dysfunction as seen in AD. Altogether, based on our *in vitro* results and these two *in vivo* studies one might speculate that other yet unidentified factors, such as inflammation, cause the barrier dysfunction as seen in AD.

Acknowledgements

This research was financially supported by Dutch Technology Foundation STW (grant no. 10703). The authors would like to thank Michelle Janssens and Julie Bekaert for their technical assistance and the personnel at the DUBBLE beam line (BM26) at the ESRF for their support with the X-ray measurements. The ceramides were kindly provided by Evonik (Essen, Germany). The project was supported by COST (European Cooperation in Science and Technology).

References

1. Simonetti O, Hoogstraate AJ, Bialik W *et al*. Visualization of diffusion pathways across the stratum corneum of native and in-vitro-reconstructed epidermis by confocal laser scanning microscopy. *Arch Dermatol Res* 1995; 287: 465-73.
2. Lampe MA, Burlingame AL, Whitney J *et al*. Human stratum corneum lipids: characterization and regional variations. *J Lipid Res* 1983; 24: 120-30.
3. Weerheim A, Ponec M. Determination of stratum corneum lipid profile by tape stripping in combination with high-performance thin-layer chromatography. *Arch Dermatol Res* 2001; 293: 191-9.
4. Wertz PW, Miethke MC, Long SA *et al*. The composition of the ceramides from human stratum corneum and from comedones. *J Invest Dermatol* 1985; 84: 410-2.
5. Bouwstra JA, Gooris GS, van der Spek JA *et al*. Structural investigations of human stratum corneum by small-angle X-ray scattering. *J Invest Dermatol* 1991; 97: 1005-12.
6. Bouwstra JA, Gooris GS, Dubbelaar FE *et al*. Phase behavior of lipid mixtures based on human ceramides: coexistence of crystalline and liquid phases. *J Lipid Res* 2001; 42: 1759-70.
7. Batheja P, Song Y, Wertz P *et al*. Effects of growth conditions on the barrier properties of a human skin equivalent. *Pharm Res* 2009; 26: 1689-700.
8. Damien F, Boncheva M. The extent of orthorhombic lipid phases in the stratum corneum determines the barrier efficiency of human skin in vivo. *J Invest Dermatol* 2010; 130: 611-4.
9. Goldsmith LA, Baden HP. Uniquely oriented epidermal lipid. *Nature* 1970; 225: 1052-3.
10. Bieber T. Atopic dermatitis. *N Engl J Med* 2008; 358: 1483-94.
11. Jakasa I, de Jongh CM, Verberk MM *et al*. Percutaneous penetration of sodium lauryl sulphate is increased in uninvolved skin of patients with atopic dermatitis compared with control subjects. *Br J Dermatol* 2006; 155: 104-9.
12. Jensen JM, Folster-Holst R, Baranowsky A *et al*. Impaired sphingomyelinase activity and epidermal differentiation in atopic dermatitis. *J Invest Dermatol* 2004; 122: 1423-31.
13. Ogawa H, Yoshiike T. A speculative view of atopic dermatitis: barrier dysfunction in pathogenesis. *J Dermatol Sci* 1993; 5: 197-204.
14. Hudson TJ. Skin barrier function and allergic risk. *Nat Genet* 2006; 38: 399-400.
15. Palmer CN, Irvine AD, Terron-Kwiatkowski A *et al*. Common loss-of-function variants of the epidermal barrier protein filaggrin are a major predisposing factor for atopic dermatitis. *Nat Genet* 2006; 38: 441-6.
16. Rodriguez E, Baurecht H, Herberich E *et al*. Meta-analysis of filaggrin polymorphisms in eczema and asthma: robust risk factors in atopic disease. *J Allergy Clin Immunol* 2009; 123: 1361-70.
17. Seguchi T, Cui CY, Kusuda S *et al*. Decreased expression of filaggrin in atopic skin. *Arch Dermatol Res* 1996; 288: 442-6.
18. van den Oord RA, Sheikh A. Filaggrin gene defects and risk of developing allergic sensitisation and allergic disorders: systematic review and meta-analysis. *BMJ* 2009; 339: b2433.
19. Janssens M, van SJ, Gooris GS *et al*. Increase in short-chain ceramides correlates with an altered lipid organization and decreased barrier function in atopic eczema patients. *J Lipid Res* 2012.
20. Cornelissen C, Marquardt Y, Czaja K *et al*. IL-31 regulates differentiation and filaggrin expression in human organotypic skin models. *J Allergy Clin Immunol* 2012; 129: 426-33, 433.
21. Howell MD, Kim BE, Gao P *et al*. Cytokine modulation of atopic dermatitis filaggrin skin expression. *J Allergy Clin Immunol* 2009; 124: R7-R12.
22. Thakoersing VS, Gooris GS, Mulder A *et al*. Unraveling barrier properties of three different in-house human skin equivalents. *Tissue Eng Part C Methods* 2012; 18: 1-11.
23. Mildner M, Jin J, Eckhart L *et al*. Knockdown of filaggrin impairs diffusion barrier function and increases UV sensitivity in a human skin model. *J Invest Dermatol* 2010; 130: 2286-94.
24. El Ghalbzouri A, Lamme E, Ponec M. Crucial role of fibroblasts in regulating epidermal morphogenesis. *Cell Tissue Res* 2002; 310: 189-99.

25. Commandeur S, Ho SH, de Gruijl FR *et al*. Functional characterization of cancer-associated fibroblasts of human cutaneous squamous cell carcinoma. *Exp Dermatol* 2011; 20: 737-42.

26. Thakoersing VS, Danso MO, Mulder A *et al*. Nature versus nurture: does human skin maintain its stratum corneum lipid properties in vitro? *Exp Dermatol* 2012; 21: 865-70.

27. de Jager M., Groenink W, Guivernau R *et al*. A novel in vitro percutaneous penetration model: evaluation of barrier properties with p-aminobenzoic acid and two of its derivatives. *Pharm Res* 2006; 23: 951-60.

28. Bligh EG, Dyer WJ. A rapid method of total lipid extraction and purification. *Can J Biochem Physiol* 1959; 37: 911-7.

29. Thakoersing VS, van SJ, Mulder AA *et al*. Increased Presence of Monounsaturated Fatty Acids in the Stratum Corneum of Human Skin Equivalents. *J Invest Dermatol* 2012.

30. Masukawa Y, Narita H, Shimizu E *et al*. Characterization of overall ceramide species in human stratum corneum. *J Lipid Res* 2008; 49: 1466-76.

31. Motta S, Monti M, Sesana S *et al*. Ceramide composition of the psoriatic scale. *Biochim Biophys Acta* 1993; 1182: 147-51.

32. de JM, Groenink W, Guivernau R *et al*. A novel in vitro percutaneous penetration model: evaluation of barrier properties with p-aminobenzoic acid and two of its derivatives. *Pharm Res* 2006; 23: 951-60.

33. van SJ, Hoppel L, van der Heijden R *et al*. LC/MS analysis of stratum corneum lipids: ceramide profiling and discovery. *J Lipid Res* 2011; 52: 1211-21.

34. Yoneda K, Nakagawa T, Lawrence OT *et al*. Interaction of the profilaggrin N-terminal domain with loricrin in human cultured keratinocytes and epidermis. *J Invest Dermatol* 2012; 132: 1206-14.

35. Aho S, Harding CR, Lee JM *et al*. Regulatory role for the profilaggrin N-terminal domain in epidermal homeostasis. *J Invest Dermatol* 2012; 132: 2376-85.

36. Irvine AD, McLean WH, Leung DY. Filaggrin mutations associated with skin and allergic diseases. *N Engl J Med* 2011; 365: 1315-27.

37. Angelova-Fischer I, Mannheimer AC, Hinder A *et al*. Distinct barrier integrity phenotypes in filaggrin-related atopic eczema following sequential tape stripping and lipid profiling. *Exp Dermatol* 2011; 20: 351-6.

38. Fallon PG, Sasaki T, Sandilands A *et al*. A homozygous frameshift mutation in the mouse Flg gene facilitates enhanced percutaneous allergen priming. *Nat Genet* 2009; 41: 602-8.

39. Oyoshi MK, Murphy GF, Geha RS. Filaggrin-deficient mice exhibit TH17-dominated skin inflammation and permissiveness to epicutaneous sensitization with protein antigen. *J Allergy Clin Immunol* 2009; 124: 485-93, 493.

40. Leisten S, Oyoshi MK, Galand C *et al*. Development of skin lesions in filaggrin-deficient mice is dependent on adaptive immunity. *J Allergy Clin Immunol* 2013; 131: 1247-50, 1250.

41. Gruber R, Elias PM, Crumrine D *et al*. Filaggrin genotype in ichthyosis vulgaris predicts abnormalities in epidermal structure and function. *Am J Pathol* 2011; 178: 2252-63.

42. Perusquia-Ortiz AM, Oji V, Sauerland MC *et al*. Complete filaggrin deficiency in ichthyosis vulgaris is associated with only moderate changes in epidermal permeability barrier function profile. *J Eur Acad Dermatol Venereol* 2013.

Supplementary Material and Methods

Primary and secondary antibodies used for immunohistochemistry
The primary antibodies used were Rabbit Filaggrin (1:1000; Covance, Rotterdam, the Netherlands), Rabbit Loricrin (1:1000; Covance, Rotterdam, the Netherlands), Mouse Ki67 (1:100; DAKO, Glostrup, Germany), Mouse Keratin 10 (1:100; Labvision / Neomarkers, Fremont CA, USA). The secondary antibodies used were biotinylated Swine anti-rabbit (1:200, DAKO), biotinylated Goat anti-Mouse (1:200, Southern Biotechnology).

Determination of the number of stratum corneum layers
Five μm sections from snap frozen NSEs were cut and stained with a 1% (w/v) safranin (Sigma) solution for 1 minute followed by 20 minutes incubation with a 2% (w/v) KOH solution to allow corneocyte swelling. Images of the sections were taken using a digital camera (Axiocam, Zeiss). The number of layers was counted in at least 6 locations covering the full length of the NSEs. This was performed for 5 different experiments.

PCR program and primers for qPCR
The PCR program was: 5 minutes at 95˚C to activate the polymerase followed by 44 cycle of 15 seconds at 95˚C, 20 seconds at 60˚C and 20 seconds at 72˚C. Afterwards a melt curve was generated. The primers used were filaggrin: forward 'GGGAAGTTATCTTTTCCTGTC' and reverse 'GATGTGCTAGCCCTGATGTTG', and β-2-microglobulin: forward 'GATGAGTATGCCTGCCGTGTG' and reverse 'CAAACCTCGGGTAGCATCAT'. Data represent the mean and standard deviation of 3 different experiments.

Western blot analysis
Protein sample was loaded onto a 10% SDS-PAGE gel and proteins were blotted on a polyvinylidene difluoride membrane (Thermo Scientific). Blocking was performed with 10% Elk Milk (Campina, The Netherlands) in phosphate-buffered saline-T (0,1% Tween). Primary antibody was incubated overnight at 4°C after which it was incubated with the appropriate secondary antibody, horseradish peroxidase-conjungated anti-rabbit (Thermo Scientific, 1:2500). Proteins were detected using Supersignal West Femto ECL (Thermo Scientific/ Pierce).

Fourier transformed infrared spectroscopy and small angle X-ray diffraction
Prior to FTIR and SAXD measurements, SC was hydrated at room temperature for 24 hours in a 27% (w/v) NaBr solution.

FTIR measurements were performed using a Varian 670-IR FTIR spectrometer (Agilent technologies, Santa Clara, CA), equipped with a broad-band mercury cadmium telluride

(MCT) detector, cooled with liquid nitrogen. The SC sample was sandwiched between AgBr windows and spectra collected in transmission mode and derived from the addition of 256 scans at 1 cm^{-1} resolution every 4 minutes (frequency range of 600-4000 cm^{-1}, temperature range of 0°C and 90°C at a rate of 0.25°C/min). Bio-Rad Win-IR Pro 3.0 software from Biorad (Biorad laboratories, Cambridge, Massachusetts) was used to process the spectra.

SAXD measurements were performed at the European Synchrotron Radiation Facility (ESRF, Grenoble) at station BM26B. A more detailed description of this beamline is described elsewhere[43]. The scattering intensity (I) was measured as a function of the scattering vector q (in nm^{-1}) defined as $q= 4\pi\sin\theta/\lambda$, in which λ is the wavelength of the X-rays and θ the scattering angle. In the generated diffraction pattern a lamellar phase is characterized by a number of equidistant peaks. The position of these peaks are directly related to the repeat distance d, $d= 2n\pi/qn$, in which n is the diffraction order and d is the repeat distance. All measurements were performed with three SC samples of all NSE types. Data represent the mean and standard deviation.

Lipid extraction

The SC lipids were extracted according to a slightly adjusted Bligh and Dyer procedure as described elsewhere[22;28]. We used a series of chloroform:methanol mixtures (1:2, 1:1, and 2:1 v/v) for 1 hour each. The extracts were combined and treated with 0.25M KCl and water. The organic phase was collected and evaporated under a stream of nitrogen at 40 °C. The obtained lipids were redissolved in a suitable volume of chloroform: methanol (2:1 v/v) and stored at −20 °C until use. To obtain enough lipids for quantification, the lipid extracts of 2-4 NSEs from each donor were pooled.

HPTLC lipid analysis and ceramide nomenclature

Ceramides with a sphingosine (S), phytosphingosine (P) or 6-hydroxysphingosine (H) are linked via an amide to a fatty acid chain, which can be either an estrified ω-hydroxy (EO), α-hydroxy (A) or nonhydroxy (N) fatty acid. The standards for HPTLC consisted of cholesterol, palmitic acid, stearic acid, arachidic acid, tricosanoic acid, behenic acid, lignoceric acid, cerotic acid, and ceramides EOS, NS, NP, EOH, and AP. All other compounds were purchased from Sigma. Lipid fractions were visualized and quantified as described before[33]. Quantification of HPTLC was performed using lipid extracts of SC from two experiments for each NSE type. Data represent mean and standard deviation of 2 different experiments.

LC/MS lipid analysis

The CERs in the pooled lipid extracts of the NSEs were analyzed using an Alliance 2695 HPLC (Waters, Milford, MA) coupled to a TSQ Quantum MS (Thermo Finnigan, San Jose, CA) measuring in APCI mode. Separation of free fatty acids was achieved using a LiChroCART Purospher STAR analytical column (55 x 2µm i.d. Merck, Darmstadt, Germany) under a flow

rate of 0.6 ml/min using a gradient system from acetonitrile/H2O to methanol/heptane. The ionization mode and scan range was altered to negative mode and 200-600 a.m.u., respectively. The total lipid concentration of all samples was around 1 mg/ml and the injection volume was set to 10 µl for the analysis of free fatty acids. Quantification of FFAs was performed using lipid extracts of SC from two experiments for each NSE type. Data represent the mean and standard deviation.

Permeability studies

In vitro permeation studies were performed with butyl para-aminobenzoic acid (butyl-PABA) as described earlier[32] using Permegear in-line diffusion cells (Bethlehem, PA, USA) with a diffusion area of 0.28 cm^2. SC was hydrated for 1 hr in PBS (pH 7.4) prior to the experiment. The donor compartment was filled with 1,5 ml butyl-PABA solution (50 µg ml^{-1} butyl-PABA) in acetate buffer (pH 5.0). The acceptor compartment consisted of PBS (pH 7.4), which was perfused at a flow rate of 1.5 ml hr^{-1}. Each experiment was performed under occlusive conditions. The temperature of the SC was maintained at 32°C during the experiment. Fractions were collected for a 15 hr time period with fixed time intervals of 1 hr. The exact volume per collected fraction was determined by weighing (balans hyperTerminal). Subsequently, the concentration of butyl-PABA in the acceptor solution was determined using HPLC as described earlier[32]. From this concentration the flux was calculated. Permeability studies were performed with at least 6 SC sheets of all NSE types. Data represent the mean ± standard error of the mean.

Supplementary Figures

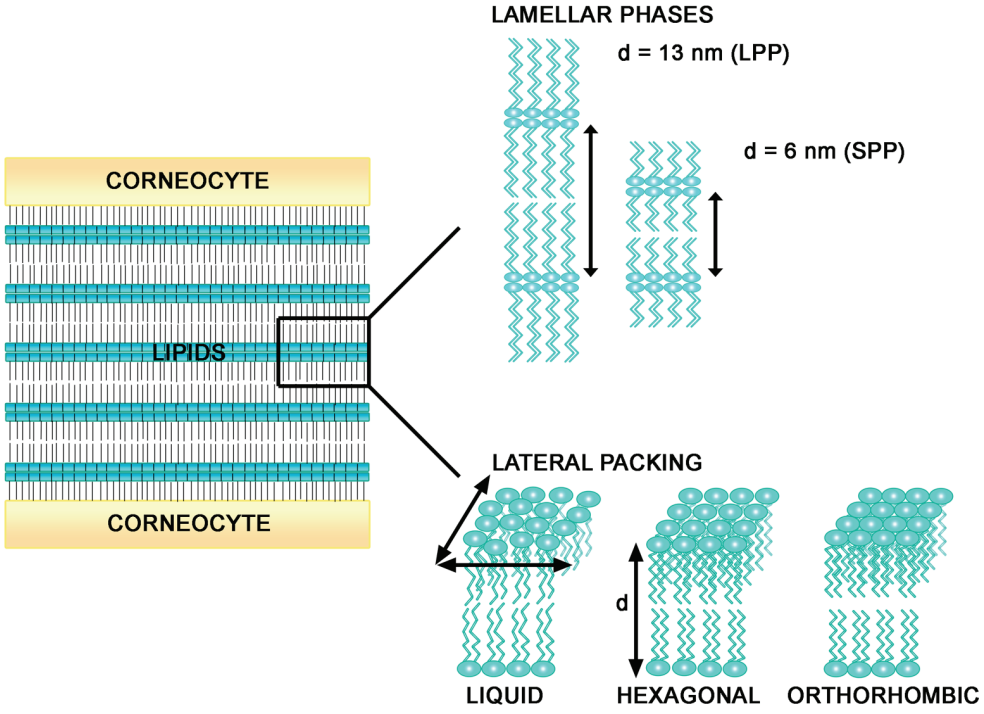

Figure S1: SC lipid organization. The SC lipids are organized into lipid lamellae, the lamellar phases. Human skin contains two lamellar phases, the long periodicity phase (LPP) and the short periodicity phase (SPP), with a repeat distance (d) of approximately 13 and 6 nm, respectively. Within the lamellar phases, the lipids are organized in a certain density, referred to as the lateral packing, either orthorhombic (very dense), hexagonal (dense) or liquid (loose). Adapted from[26].

a

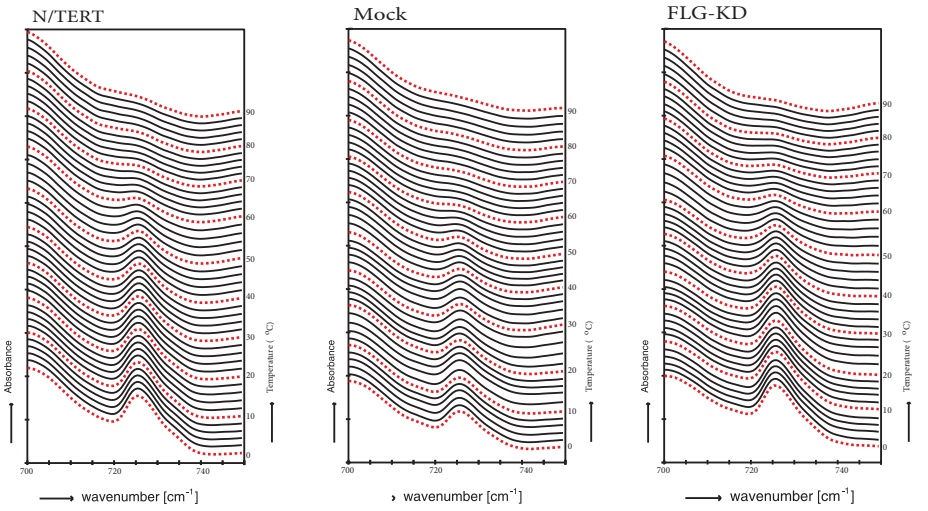

b

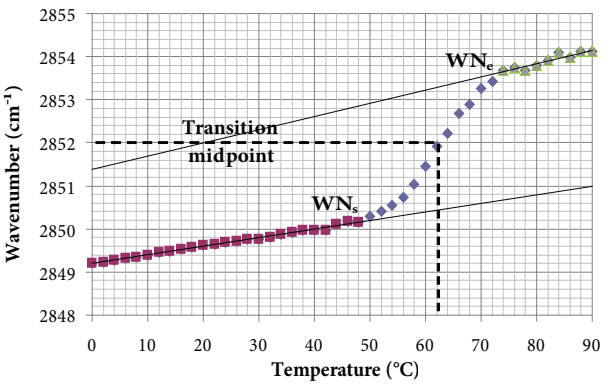

c

Sample	Order-Disorder Transition	Symm stretch (cm^{-1}) at 32°C
N/TERT	57,3 ± 2,3°C	2850,3 ± 0,2
Mock	54,3 ± 0,6°C	2850,7 ± 0,6
FLG-KD	55 ± 1°C	2850,8 ± 0,8

Figure S2: Effect of FLG-KD on the lateral packing of SC lipids. (a) Representative rocking vibrations in a temperature range from 0-90°C in N/TERT, Mock and FLG-KD NSEs. All NSEs show hexagonal packing indicating that knockdown of filaggrin did not affect the lateral packing. (b) the CH_2 symmetric stretching wavenumbers are plotted as a function of temperature. In this example the calculation of the midpoint temperature of the order-disorder transition. Adapted from[22]. (c) The midpoint order-disorder transition temperature and the symmetric stretching frequencies at 32˚C, which corresponds to the *in vivo* skin temperature. FLG-KD did not affect the midpoint order-disorder transition temperature nor the symmetric stretching frequencies compared to Mock HSEs. Data represent mean ± SD of 3 independent experiments.

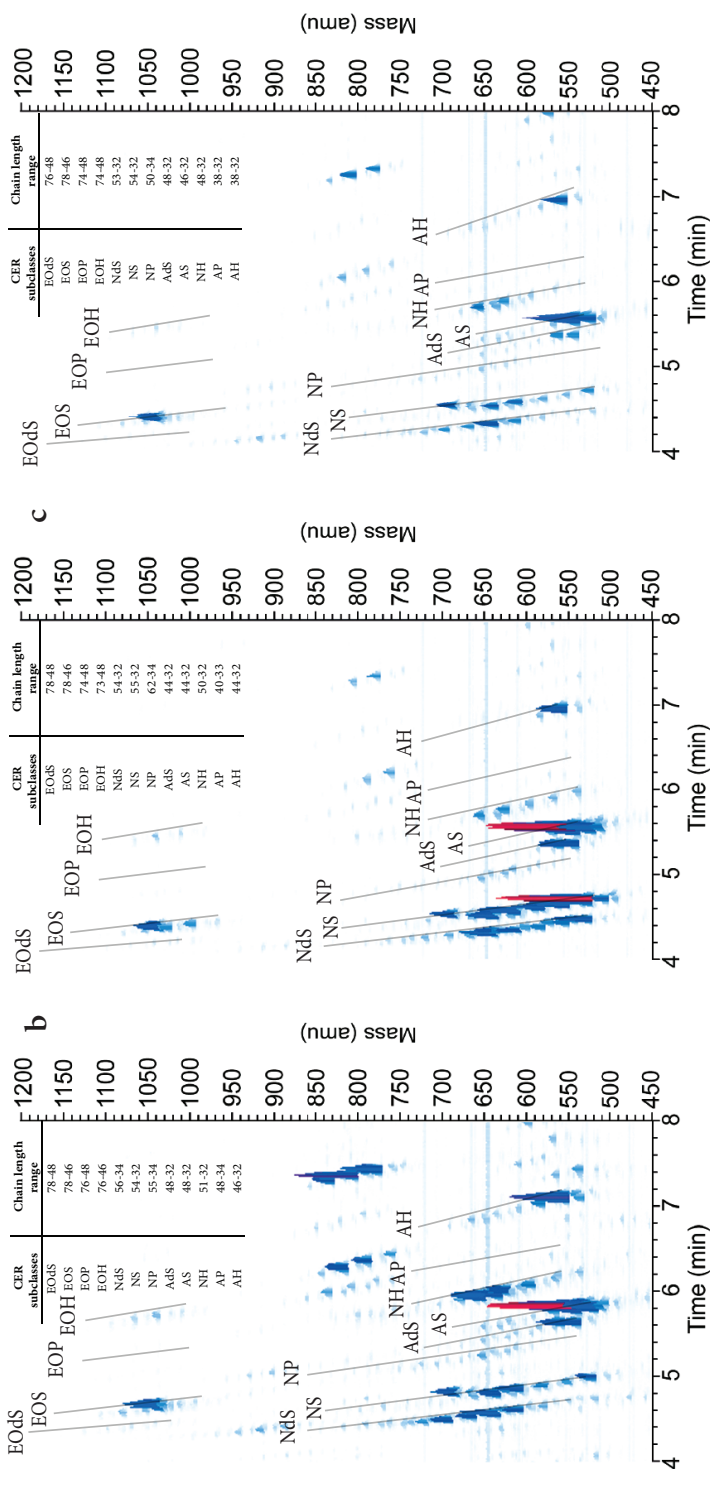

Figure S3: Liquid chromatography/mass spectrometry (LC/MS) chromatograms. Three-dimensional multi-mass LC/MS chromatogram of the CERs present in SC lipid extracts from (a) N/TERT, (b) Mock and (c) FLG-KD NSEs. Presence and chain length distribution of the 12 CER subclasses was not affected by FLG-KD.

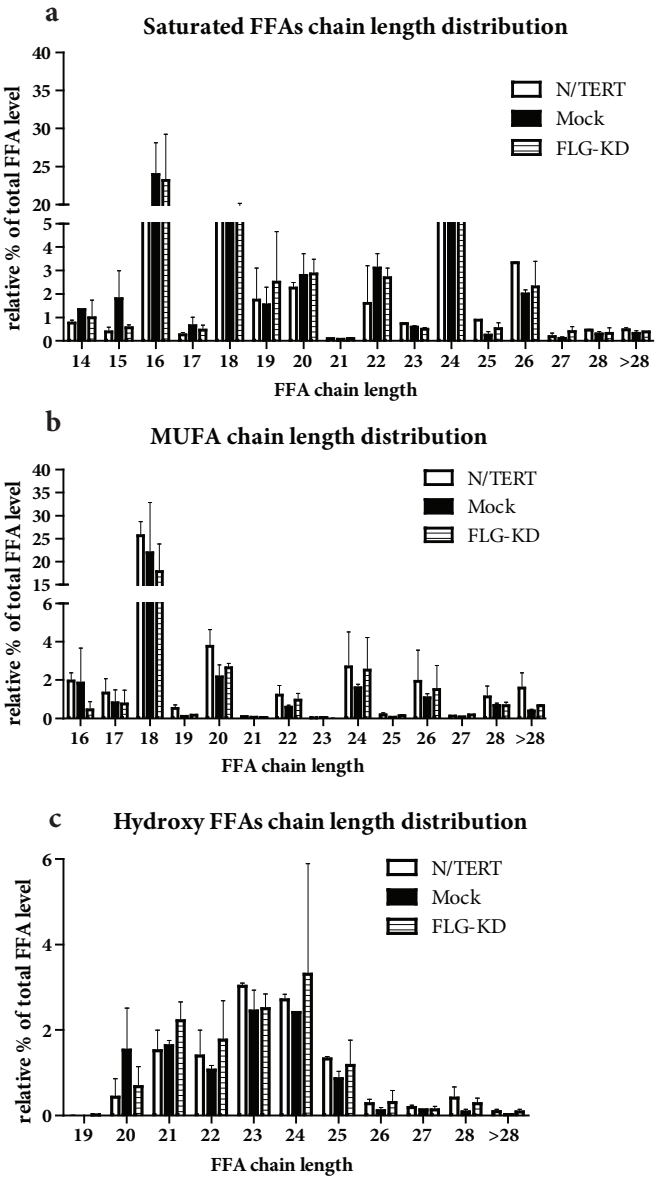

Figure S4: quantification of the SC FFAs. (a-c) Chain length distribution of saturated FFA, mono unsaturated FFAs (MUFAs) and hydroxyl FFAs, respectively. The FFA chain length distribution of the saturated FFA, MUFAs and hydroxyl FFAs was not affected by FLG-KD.